Available online at www.sciencedirect.com
ScienceDirect
Journal of the European Ceramic Society 27 (2007) 3677–3682
www.elsevier.com/locate/jeurceramsoc

Structural characterization of $Ce_{1-x}Zr_xO_2$ ($0 \leq x \leq 1$) samples prepared at 1650 °C by solid state reaction A combined TEM and XRD study

A. Varez [a,*], E. Garcia-Gonzalez [b], J. Jolly [a,c], J. Sanz [c]

[a] *Dpto. Materiales, Escuela Politécnica Superior, Universidad Carlos III de Madrid, 28911 Leganés, Spain*
[b] *Dpto. Química Inorgánica, Facultad Ciencias Químicas, Universidad Complutense de Madrid, 28040 Madrid, Spain*
[c] *Instituto Ciencia de Materiales, CSIC, Cantoblanco, 28049 Madrid, Spain*

Available online 19 March 2007

Abstract

In this paper we present the structural study of the $Ce_{1-x}Zr_xO_2$ ($0 \leq x \leq 1$) samples, prepared at 1650 °C by solid state reaction. The study was performed by means of powder X-ray diffraction (XRD) and selected area electron diffraction (SAED) techniques. The Rietveld analysis of XRD patterns shows that all the samples adopt the fluorite structure although with different symmetries. In the Zr-rich area ($x > 0.8$) the monoclinic phase (S.G. $P2_1/c$) is detected, while in the Ce-rich area the cubic solid solution (S.G. Fm-$3m$) is stabilized in a wide compositional range ($0 \leq x \leq 0.4$). For $x = 0.5$, the metastable tetragonal T′ phase is detected as unique phase. In the intermediate region ($0.6 \leq x \leq 0.8$), XRD patterns are formed by those of the stable cubic and tetragonal T phases besides that of the metastable T′ phase (S.G. $P4_2/nmc$). Through the Rietveld analysis, sites occupation and relative percentages of different phases have been determined. Cation miscibility was investigated by means of selected area electron diffraction (SAED) combined with EDS microanalysis at the nanoscale level. Solubility ranges deduced are discussed in terms of phase diagrams previously reported.

Keyword: CeO_2; ZrO_2; Powder-solid state reaction; X-Ray methods; Fuel cells; TEM

1. Introduction

CeO_2–ZrO_2 mixed oxides are attractive materials used as structural ceramics with high toughness, in fuel cells, oxygen sensors, etc.[1–3] Their physico-chemical properties depend on the crystal structure, composition and microstructure. Partially stabilized zirconia are interesting materials for structural and mechanical applications, while Ce-rich fully stabilized zirconia are interesting for electrochemical applications. Finally, Ce–Zr oxides are promising materials in heterogeneous catalysis because of its high oxygen storage capacity and thermal stability.[3]

The most accepted phase diagram was proposed by Yashima et al.[4] on the basis of samples prepared by the solid state reaction method. In the Ce-rich area (above 80 mol%) a cubic phase (S.G. Fm-$3m$) was detected, while below 20 mol% monoclinic (S.G. $P2_1/c$) and/or tetragonal phases (S.G. $P4_2/nmc$) were stabilized. At intermediate compositions (20–80 mol%), Yashima et al.[4,5] proposed the existence of three tetragonal phases, T, T′ and T″. These phases present the same space group $P4_2/nmc$, but different tetragonal distortion ($c/a = 1.02$, 1.001–1.02 and 1, respectively). At high temperatures, the T phase is stable while T′ and T″ are metastable.

In the present contribution, the solubility range in CeO_2–ZrO_2 system has been investigated in samples prepared by the solid state reaction at 1650 °C. Crystal by crystal EDS analysis performed on these samples has shown a higher Ce–Zr solubility at the atomic level than that reported for samples prepared at 1500 °C.[6] Structural features of different phases have been deduced from the Rietveld analysis of XRD patterns. Finally, the phase percentage and cation solubility of each phase have been determined.

2. Experimental

Appropriate quantities of CeO_2 (99.9% Aldrich) and ZrO_2 (Aldrich 99.9%) powders were mixed in an agate mortar to

* Corresponding author at: Avda. Universidad, 30, 28911 Leganés, Madrid, Spain. Tel.: +34 916249484; fax: +34 916249430.
E-mail address: alvar@ing.uc3m.es (A. Varez).

0955-2219/$ – see front matter © 2007 Elsevier Ltd. All rights reserved.
doi:10.1016/j.jeurceramsoc.2007.02.014

prepare oxides of the $Ce_{1-x}Zr_xO_2$ series ($0 \le x \le 1$). Mixtures were consolidated by cold isostatic pressure and heated at 1650 °C during 24 h. From that temperature samples were slowly cooled to room temperature (1 °C/min). Samples were never reheated or annealed at intermediate temperatures.

Powder X-ray diffraction (XRD) experiments were carried out on a Philips X'Pert-MPD diffractometer ($\theta/2\theta$ Bragg-Brentano geometry) with a Cu Kα radiation by working at 40 kV and 40 mA. Patterns were recorded on a 2θ range of 20–120°, with the step-scanning mode (0.02° step); 8 s of counting time; 1° divergence slit; 1° anti-scatter slit and 0.1 mm receiving slit.

The Rietveld refinement of XRD patterns was carried out by using the Fullprof program.[7] On a first stage, zero corrections, scaling factors, unit cell parameters, shape peak parameters (including FWHM, asymmetry and pseudo-voigt profile functions) were determined. On a second step, isotropic thermal factors, atomic coordinates and site occupancies were deduced.

Samples for transmission electron microscopy were ultrasonically dispersed in *n*-butanol and transferred to carbon coated copper grids. Selected area electron diffraction (SAED) patterns were taken on a PHILIPS CM20 FEG SuperTwin electron microscope equipped with an EDAX analyzer DX4 (Super Ultra Thin window (resolution ≈135 eV). With this technique crystal by crystal Ce/Zr ratios were determined.

3. Results and discussion

3.1. X-ray diffraction

Fig. 1 shows XRD patterns of different $Ce_{1-x}Zr_xO_2$ compositions prepared at 1650 °C by solid state reaction. The patterns have been separated in three groups in order to discuss about the different detected phases. In Ce-rich compositions ($x \le 0.4$), only reflections of the cubic fluorite have been found (Fig. 1a). These peaks are shifted to higher 2θ values as a consequence of the substitution of Ce^{4+} ($r^{VIII} = 0.97$ Å) by smaller Zr^{4+} ions ($r^{VIII} = 0.84$ Å).[8] Zr incorporation produces the contraction of the cubic unit cell from 5.4113(1) to 5.3110(1) Å when x increases from $x = 0$ to $x = 0.4$. In the case of the sample with $x = 0.5$, observed peaks correspond to the unit cell of the tetragonal T′ phase, $a = 3.7222(1)$ Å and $c = 5.3109(1)$ Å.[5,9,10]

For $0.6 \le x \le 0.8$ compositions, XRD patterns display diffraction peaks of three different phases: one cubic (C) and two tetragonal (T and T′) with different *c*/*a* ratio (Fig. 1b). The intensity of the main peaks of each phase changes with the composition. In particular the most intense peaks of T′ and T phases, located at $2\theta \approx 30°$, decrease and increase, respectively as the Zr content increases. Finally in Zr-rich samples ($x = 0.9$ and 1), the monoclinic m-ZrO_2 phase was preferentially formed (Fig. 1c). The peaks of the m-ZrO_2-doped sample are better resolved than those of pure ZrO_2, indicating that the incorporation of Ce increases the crystallinity of this phase.

The Rietveld analysis of the different samples was carried out in order to determine the structural changes produced by the substitution of Ce by Zr. The refinement of X-ray diffraction patterns of the series $Ce_{1-x}Zr_xO_2$ ($0 \le x \le 1$) was successfully performed using cubic, tetragonal and monoclinic reported

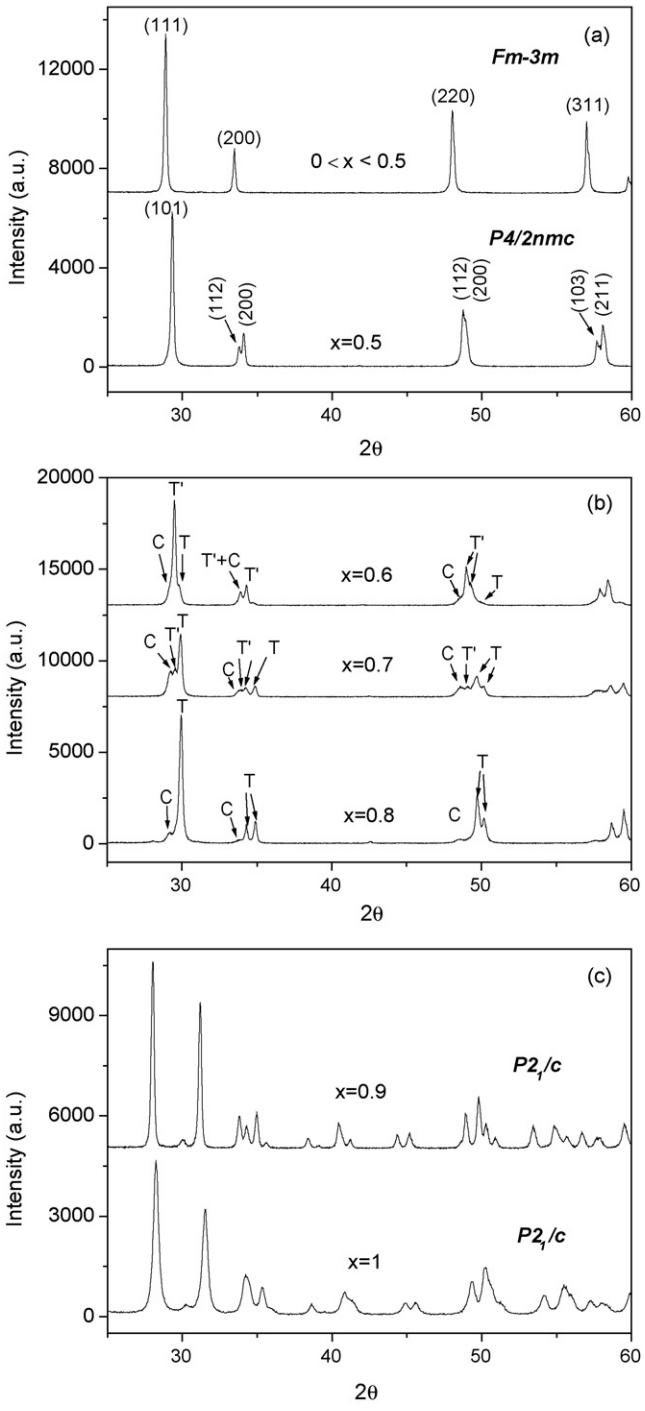

Fig. 1. XRD patterns of $Ce_{1-x}Zr_xO_2$ samples prepared at 1650 °C by solid state reaction. Miller indices of the most intense peaks of cubic (C), tetragonal (T and T′) and monoclinic (M) phases are indicated.

models.[1] In multiphase region, isotropic thermal factors of cations become negative. This effect has been often associated with microabsorption processes in polyphasic samples.[11] To avoid this problem, thermal factors were fixed to those of the pure phases. In Fig. 2, the results of the refinements of $Ce_{0.5}Zr_{0.5}O_2$ and $Ce_{0.2}Zr_{0.8}O_2$ samples are given as examples. In the first case, the tetragonal T′ phase was the unique detected phase.[10] In the second case, the presence of C, T and T′ phases were

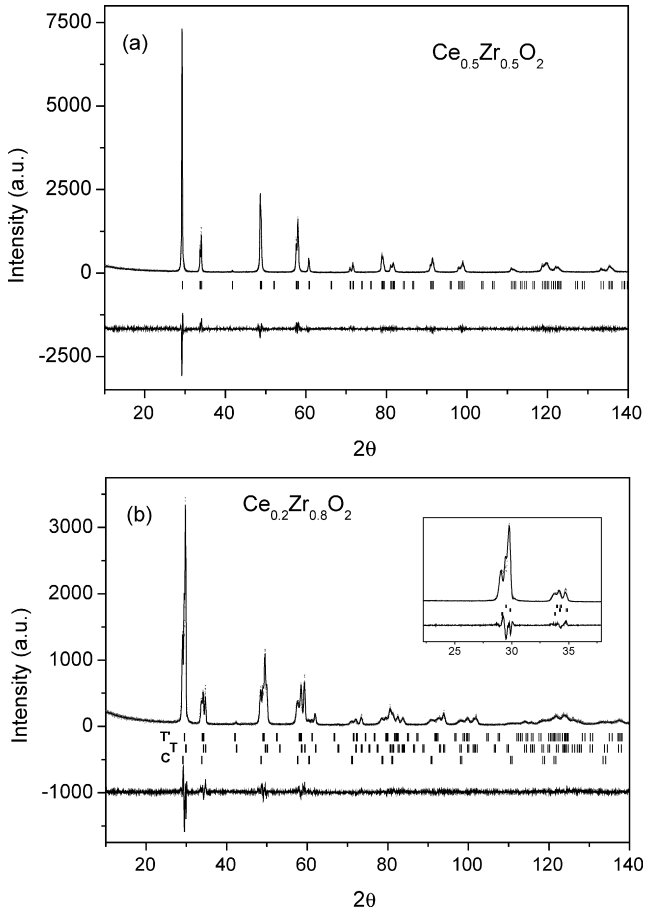

Fig. 2. Rietveld analysis of X-ray diffraction patterns of (a) $Ce_{0.5}Zr_{0.5}O_2$ and (b) $Ce_{0.2}Zr_{0.8}O_2$ samples. Bragg positions of different phases are given. Differences between observed and calculated intensities are included at the bottom of the figure.

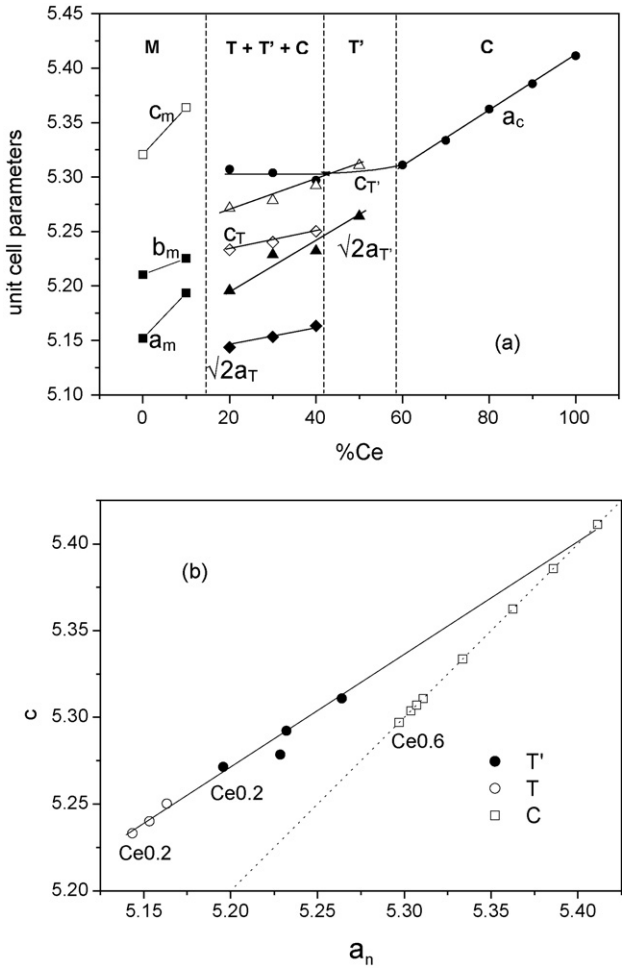

Fig. 3. (a) Dependence of lattice parameters on the Ce content of $Ce_{1-x}Zr_xO_2$ samples. (b) Variation of a and c parameters in C, T and T′ phases. The tetragonal unit cell parameter, a(T), has been normalized to the ideal cubit unit cell to favour the comparison (a_n(T) = a(T) ∗ $\sqrt{2}$).

detected. A summary of structural parameters and agreement factors obtained in this analysis is given in Table 1.

Fig. 3a shows the dependence of unit cell parameters on the Ce content for the different phases. In the cubic region, the lattice parameters of the CeO_2 fluorite decrease progressively as the Zr content increases ($0 \leq x \leq 0.4$). In the multiphase region, the unit cell parameters of the cubic and tetragonal T phases remain almost constant, but those of the tetragonal T′ phase change in a significant way. In monoclinic samples ($0.8 \leq x \leq 1$), unit cell parameters increase with the Ce content and the **a** and **b** unit cell parameters approach a single value. In these samples, the β angle decreases also with the Ce content. Similar results were found in samples heated at 1500 °C; however, in this case the tetragonal T′ phase was not detected.[6]

In Fig. 3b, unit cell parameters of different compositions (renormalized to those of the cubic fluorite phase) are analyzed without regarding the composition of samples. In the case of cubic phases, the slope of the curve is obviously one and the accumulation of points at $a = 5.325$ Å, suggests that composition of the cubic phase does not change further in the $0.6 \leq x \leq 0.8$ region. In the case of the tetragonal T and T′ phases, unit cell parameters are located in the same straight line, suggesting that structural distortions disappear progressively when the Ce content increases. The accumulation of points at $a_n = 5.160$ and $c_n = 5.240$ Å, indicates again that the composition of the tetragonal T phase does not significantly change in the compositional range $0.6 \leq x \leq 0.8$ (Table 1). In the same compositional range, unit cell parameters and composition of the T′ phase change appreciably.

Structural site occupancies have been analyzed in different crystalline phases (Table 1). In cubic samples (S.G. *Fm*-3*m*), the occupancy of 4a site by Zr ions increases as the Zr content increases up to the $Ce_{0.6}Zr_{0.4}O_2$. In the multiphasic region where cubic and two tetragonal phases coexist (20–40% of CeO_2), the occupancy of 4a site of *Fm*-3*m* and 2a site of the T phase (S.G. $P4_2/nmc$), remain almost constant, while in the case of the T′ phase the composition goes from $Ce_{0.5}Zr_{0.5}O_2$ to $Ce_{0.3}Zr_{0.7}O_2$. In this compositional region, the cubic phase present a composition close to $Ce_{0.6}Zr_{0.4}O_2$, while, the tetragonal phase is always close to $Ce_{0.2}Zr_{0.8}O_2$. These values agree with variations detected on the unit cell parameters of these phases (Fig. 3a). Site occupation also changes slightly with the Ce content in the monoclinic phase, attaining the values of the tetragonal phase ($Zr_{0.8}Ce_{0.2}$).

Table 1
Structural parameters deduced from Rietveld refinement of the X-ray diffraction patterns for $Ce_xZr_{1-x}O_2$ ($0 \le x \le 1$) samples

S.G./x		0	0.1	0.2	0.3	0.4	0.5	0.6	0.7	0.8	0.9	1
$P2_1/c$	a_m	5.1514(4)	5.1934(2)									
	b_m	5.2098(4)	5.2254(2)									
	c_m	5.3204(4)	5.3639(2)									
	β	99.171(3)	98.974(2)									
	x (Zr)	0.2756(3)	0.2735(2)									
	y (Zr)	0.0388(3)	0.0367(2)									
	z (Zr)	0.2092(3)	0.2092(2)									
	x (O1)	0.068(2)	0.069(2)									
	y (O1)	0.327(2)	0.318(2)									
	z (O1)	0.339(2)	0.352(2)									
	x (O2)	0.448(2)	0.456(2)									
	y (O2)	0.761(2)	0.757(2)									
	z (O2)	0.479(2)	0.472(2)									
	Ce (occ)	0	0.19(2)									
	R_B	5.16	8.55									
	% phase	100	100									
$P4_2/nmc$ T′	a_t			3.6740(1)	3.6972(1)	3.6997(1)	3.7222(1)					
	c_t			5.2715(1)	5.2785(1)	5.2922(1)	5.3109(1)					
	z (O)			0.459(2)	0.4529(2)	0.4618(2)	0.463(2)					
	Ce (occ)			0.66(7)	0.58(7)	0.62(5)	0.50(3)					
	R_B			15.6	5.03	4.51	7.67					
	% phase			11.2	21.29	73.16	100					
$P4_2/nmc$ T	a_t			3.6371(1)	3.6439(1)	3.6510(1)						
	c_t			5.2332(1)	5.2401(1)	5.2502(1)						
	z (O)			0.452(2)	0.452(2)	0.455(2)						
	Ce (occ)			0.17(4)	0.18(5)	0.18(7)						
	R_B			8.65	4.71	6.51						
	% phase			82.48	54.76	12.24						
Fm-3m	a_c			5.3071(1)	5.3039(1)	5.2970(1)		5.3110(1)	5.3337(1)	5.3619(1)	5.3857(1)	5.4113(1)
	Ce (occ)			0.67(7)	0.67(6)	0.67(7)		0.62(6)	0.69(6)	0.81(5)	0.91(4)	1.00(2)
	R_B			33.6	5.08	4.52		12.6	9.60	8.47	9.61	3.20
	% phase			6.32	23.95	14.60		100	100	100	100	100
	R_p	8.09	11.9	13.9	11.9	9.39		16.1	14.9	12.4	13.3	9.41
	R_{wp}	10.4	15.1	18.5	16.2	13.0		21.2	18.8	16.8	16.0	14.1
	χ^2	2.37	3.78	2.11	3.95	1.43		4.77	4.67	4.87	4.58	2.24

Finally, the relative amounts of different phases have been determined (Table 1). In Ce and Zr rich samples, cubic and monoclinic single phases were observed in which cation miscibility was detected. In the multiphasic $0.5 \leq x \leq 0.8$ region, compositions of the cubic C and the tetragonal T phases do not change appreciably; but, relative percentages of two phases change in a significant way. However, composition of the T′ phase change considerably in this region, decreasing the relative phase percentage as the Zr content increases (Table 1).

3.2. Electron diffraction

In order to study the microstructural aspects of the samples, SAED has been performed. This study has been combined with a crystal by crystal EDS microanalysis, to determine the chemical composition of individual crystallites. It is important to remark that for single phase samples, a very good agreement was obtained between nominal and deduced compositions.

As a general trend, the electron diffraction study confirmed the results obtained by powder X-ray diffraction. For the Zr-rich samples, homogeneous crystals are formed which crystallize in the m-ZrO_2 type phase. Fig. 4a corresponds to the SAED pattern of a crystal of composition $Ce_{0.1}Zr_{0.9}O_2$ taken along the $[1\,0\,0]_m$ zone axis (Miller index refer to the m-ZrO_2 type phase, space group $P2_1/c$).

For the $x = 0.5$ composition, a single phase with tetragonal symmetry is detected, the Ce:Zr ratio being 1:1 in all the investigated crystals. Fig. 4b shows the SAED pattern of a crystal of $Ce_{0.5}Zr_{0.5}O_2$ taken along the $[0\,1\,0]_t$ zone axis (Miller index refer to the t-ZrO_2 phase, space group $P4_2/nmc$).

In the Ce-rich region ($0.4 \leq x \leq 0.1$) electron diffraction shows the existence of crystals with cubic and tetragonal symmetry. Fig. 4c shows the SAED pattern of a crystal of composition $Ce_{0.8}Zr_{0.2}O_2$. As it can be observed, extra spots in respect to the cubic cell, can be assigned according to the same symmetry in both Fig. 4b and c. However, the diffuse aspect of the extra maxima in Fig. 4c allow us to assign the diagram to the tetragonal T″ phase.[6,12] In this phase, the tetragonal distortion comes from oxygen atoms displacement. This phase, not observed in XRD patterns, was also detected in Ce-rich samples prepared at $T = 1500\,^{\circ}C$.[6]

3.3. Phases metastability

In this work, two metastable tetragonal (T′ and T″) and three stable phases (C, T and M) have been detected by XRD and SAED techniques in $Ce_{1-x}Zr_xO_2$ samples prepared at 1650 °C. The relative amount of these phases changes with the composition. The cubic phase is stabilized in most part of compositions ($x \geq 0.6$). However, in $x = 0.5$ sample, the cooling rate used favoured the formation of the metastable T′ phase. In samples with $0.2 \leq x \leq 0.5$, the formation of cubic and tetragonal T phases was detected besides that of the T′ phase. These results are in agreement with previous published works, in which it was shown that the annealing of the T′ phase at increasing temperatures produced the transformation of T′ into C + T phases.[13] However, a comparison of described results with those deduced from phase diagrams, cannot be undertaken because the presence of metastable T′ and T″ phases. In the last case, the differentiation of the tetragonal T″ and the cubic C phases, can only be achieved with SAED or Raman techniques. Unfortunately, the quantification of different phases is difficult with these techniques.

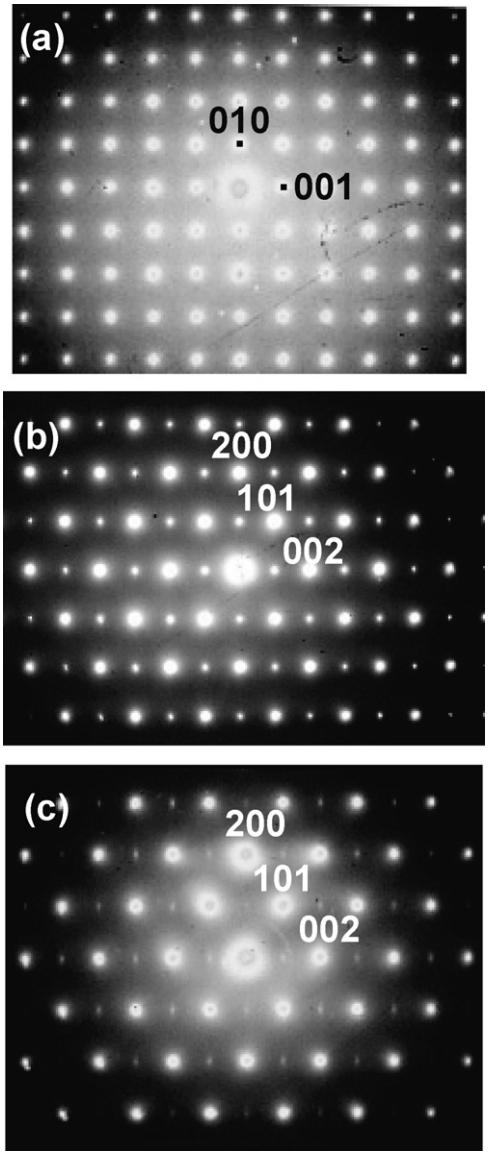

Fig. 4. Selected area electron diffraction patterns (SAED) of crystals with composition: (a) $Ce_{0.1}Zr_{0.9}O_2$, (b) $Ce_{0.5}Zr_{0.5}O_2$ and (c) $Ce_{0.9}Zr_{0.1}O_2$ (see text for discussion).

4. Conclusions

Structure and cation miscibility have been investigated in $Ce_{1-x}Zr_xO_2$ samples through the Rietveld analysis of XRD patterns. The structure of individual crystallites has also been analyzed by means of TEM and SAED techniques. The main results are summarized as follows:

(1) A good miscibility was found in cubic Ce-rich $Ce_{1-x}Zr_xO_2$ samples ($0 \leq x \leq 0.4$). However the TEM analysis showed

that cubic and tetragonal T″ phases coexist in Ce rich samples.

(2) The T′ phase was obtained as single phase for the $Ce_{0.5}Zr_{0.5}O_2$ composition.

(3) In the multiphasic $0.6 \leq x \leq 0.8$ region, T and T′, phases coexist with the cubic C phase. The T′ changes into the C + T phases as the Zr content increases.

(4) The monoclinic M phase is present in the Zr rich area ($x > 0.8$) as a single phase. The crystallinity of these samples improves with the Ce content.

The Rietveld analysis of XRD patterns has also been successfully applied to determine relative percentages of detected phases in the multiphasic region. Structural sites occupation deduced with this technique is in agreement with the variations detected on unit cell parameters of these phases.

Acknowledgements

Authors thank Dr. M.L. Sanjuan for their helpful discussions and comments. Spanish Agency CICYT (projects MAT2004-03070-C05-02 and MAT2004-01248) and the regional Government of Madrid (project S-505/PPQ-0358) are gratefully acknowledged for financial support.

References

1. Kaspar, J. and Fornasiero, P., *Catalysis by Ceria and Related Materials*, *Vol 2*, ed. A. Trovarelli. Catalytic Science Series, 2002, pp. 217–241 (Chapter 6).
2. Di Monte, R. and Kaspar, J., Nanostructure CeO_2–ZrO_2 mixed oxides. *J. Mater. Chem.*, 2005, **15**, 633–648.
3. Kaspar, J. and Fornasiero, P., Nanostructured materials for advanced automotive de-pollution catalysts. *J. Solid State Chem.*, 2003, **171**, 19–29.
4. Yashima, M., Arashi, H., Kakihana, M. and Yoshimura, M., Raman scattering study of cubic-tetragonal phase transition in $Zr_{1-x}Ce_xO_2$ solid solution. *J. Am. Ceram. Soc.*, 1994, **77**, 1067–1071.
5. Yashima, M., Takashina, M., Kakihana, M. and Yoshimura, M., Low-temperature phase equilibria by the flux method and the metastable-stable phase diagram in the ZrO_2–CeO_2 system. *J. Am. Ceram. Soc.*, 1994, **77**, 1869–1874.
6. Varez, A., Garcia-González, E. and Sanz, J., Cation miscibility in CeO_2–ZrO_2 oxides with fluorite structure. A combined TEM, SAED and XRD Rietveld analysis. *J. Mater. Chem.*, 2006, **16**, 4249–4256.
7. Rodríguez-Carvajal, J., Recent advances in magnetic-structure determination by neutron powder diffraction. *Physica B*, 1992, **192**, 55–69 (Fullprof Program: Rietveld Pattern Matching Analysis of Powder Patterns, Grenoble, ILL, 1990).
8. Kaspar, J., Fornasiero, P. and Graziani, M., Use of CeO_2-based oxides in the three-way catalysis. *Catal. Today*, 1999, **50**, 285–298.
9. Yashima, M., Morimoto, K., Ishizawa, N. and Yoshimura, M., Diffusionless tetragonal-cubic transformation temperature in zirconia–ceria solid solutions. *J. Am. Ceram. Soc.*, 1993, **76**, 2865–2868.
10. Otsuka-Yao-Matsuo, S., Yao, T. and Omata, T., Thermodynamic stability of metastable tetragonal t′-$Ce_{0.5}Zr_{0.5}O_2$ phase in the CeO_2–ZrO_2 system. *High Temp. Mater. Process.*, 2003, **22**, 157–164.
11. Young, R. A., *"The Rietveld Method" International Union of Crystallography*. Oxford University Press, 1993;
Smith, D. K., Johnson Jr., G. G., Scheible, A., Wims, A. M., Johnson, J. L. and Ullman, G., *Powder Diffraction*, 1987, **2**, 73–77.
12. Colón, G., Pijolat, M., Valdivieso, F., Vidal, H., Kaspar, J., Finocchio, E. *et al.*, Surface and structural characterization of $Ce_xZr_{1-x}O_2$ CEZIREN-CAT mixed oxides as potential three-way catalyst promoters. *J. Chem. Soc., Faraday Trans.*, 1998, **94**, 3717–3726.
13. Yashima, M., Morimoto, K., Ishizawa, N. and Yoshimura, M., Zirconia–ceria solid solutions synthesis and the temperature-time-transformation diagram for the 1:1 composition. *J. Am. Ceram. Soc.*, 1993, **76**, 1745–1750.